Electronic Supplementary Material (ESI) for Chemical Communications.

Towards the tailored design of benzotriazinyl-based organic radicals displaying a spin transition

Maria Fumanal,[a] Sergi Vela, [ab]* Juan J. Novoa[a] and Jordi Ribas-Ariño[a]

[a]Departament de Química Física and IQTCUB, Facultat de Química, Universitat de Barcelona, Av. Diagonal 645, 08028 Barcelona, Spain.

[b]Laboratoire de Chimie Quantique, Institut de Chimie UMR 7177, Université de Strasbourg, Strasbourg, France.

*sergi.vela@gmail.com

-Supporting Information-

Supp. Section S1 – Crystal structure and definition of the structural parameters that characterize the dimers

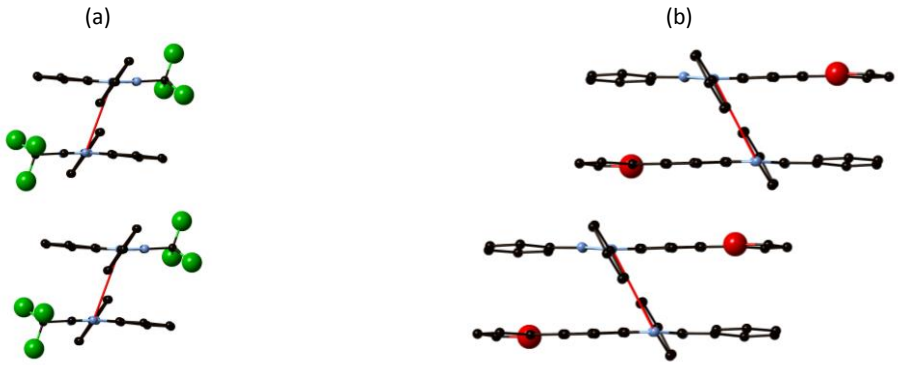

Figure S1a. Stacks of monomers of (a) compound **1** at 75 K and (b) of compound **2** at the crystal structure resolved at 100 K. Hydrogen atoms are omitted for clarity. Along the manuscript, the discussion is based on the spin state of the dimers highlighted with a red line.

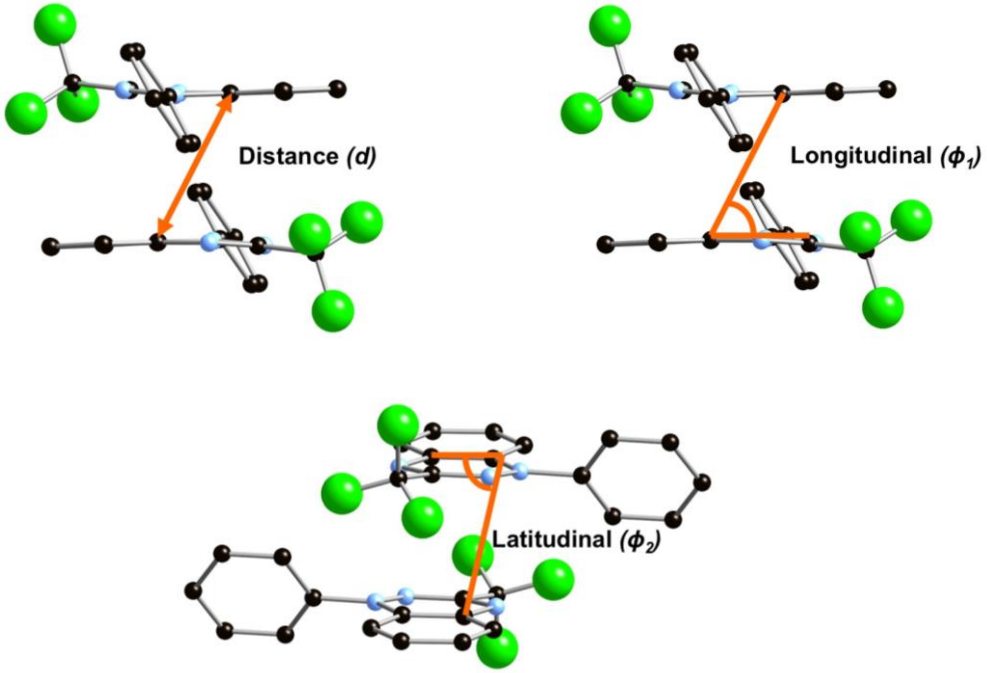

Figure S1b. Definition of the structural parameters distance (d), longitudinal angle (ϕ_1) and latitudinal angle (ϕ_2) used to characterize the dimer along the stacking direction. Hydrogen atoms have been hidden for clarity.

Supp. Section S2 – Computational details and model systems for the calculations in the solid state

When working in the crystalline phase, the minimum energy structures of compounds **1** and **2** were obtained through variable-cell geometry optimizations, in which the size and shape of the unit cell was allowed to change. Those were first obtained using supercells formed by two columns of four radicals in its crystal-structure coordinates (see Figure S2a). For these calculations, the Γ-point sampling of the Brillouin zone was employed. Then, to confirm the presence of two different minima in the potential energy surface of the HS state of compound **1**, a second supercell containing four columns of two radicals in its crystal-structure was used (see Figure S2b). In this case, a 1x4x1 grid of K-points was used in the sampling of the Brillouin zone in order to properly describe the propagation in the stacking direction. The use of both types of supercells yielded the same minima. Finally, we must note that we have used the spin state of the individual dimers when defining the spin state of the different minima in the solid state. That is, in **1**-HT^{HS}, **1**-LT^{HS} or **2**^{HS}, where the Pair-I dimers are in its triplet HS state, the total spin of the whole unit cell, which contains 8 molecules, is S=4.

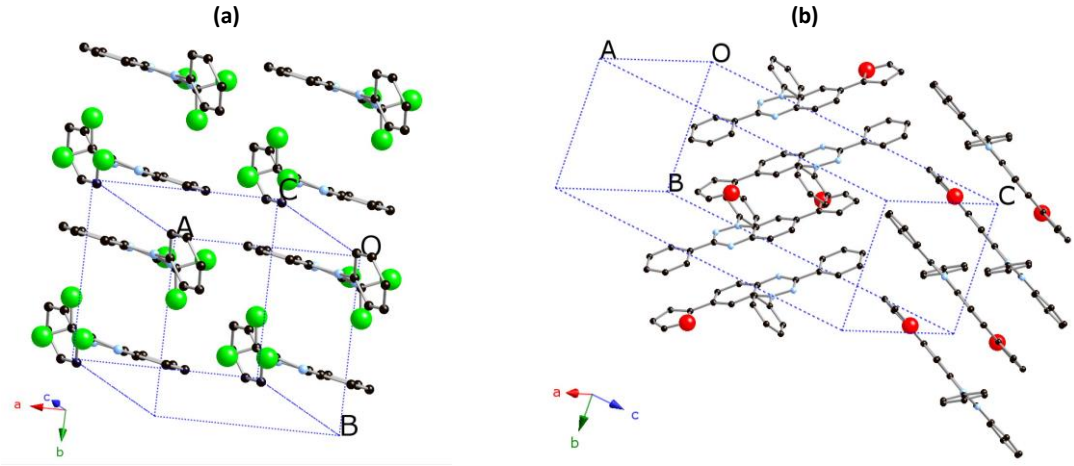

Figure S2a. Supercells used as the unit cell for the variable-cell optimizations of systems (a) **1** and (b) **2**.

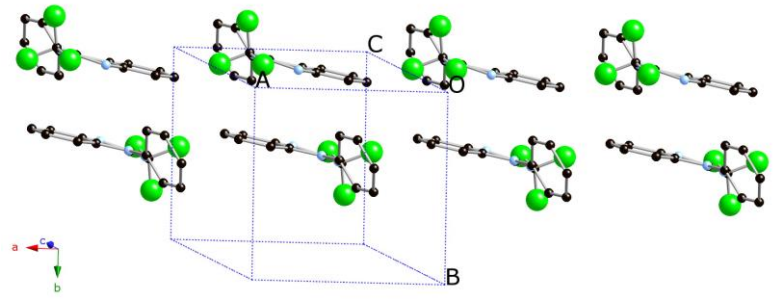

Figure S2b. Alternative supercell used as the unit cell for the variable-cell optimizations of the HS state of system **1**.

All the calculations in the crystalline phase were carried out in three-dimensional periodic boundary conditions using the Quantum Espresso code.[1] The Perdew-Burke-Ernzerhof (PBE) functional,[2, 3] within the spin unrestricted formalism, together with the Vanderbilt ultrasoft pseudopotentials and the DFT-D2 parametrization of the Grimme's dispersion correction[4] was employed. The plane-wave kinetic energy cutoff was set to 70 Ry. The number of plane waves was kept constant throughout the variable-cell relaxations. A constant number of plane waves implied no Pulay stress, but a decreasing precision of the calculation as the volume of the supercell increased. However, the large cutoff employed in these calculations ensured that the artifacts arising from this change of precision were negligible. A series of recent benchmark calculations showed that the use of PBE, together with the Grimme correction, gives good predictions of the structure and cohesive energies of the molecular crystals.[5] The vibrational modes could not be calculated because of the huge computational requirements needed to perform such task: each cell consisted on 232 and 344 atoms for **1** and **2**, respectively, and thus, the finite differences technique would have required 1392 and 2064 calculations. Since three and two minima were obtained in the solid state for **1** and **2**, we would have needed a total of 8304 energy and gradient evaluations.

Supp. Section S3 - Minima of the HS- and LS- Potential Energy Surfaces in the Solid State

For compound **1**, its LT- and HT- X-ray crystal structures have been taken as the initial nuclear coordinates for a variable-cell optimization procedure. The resulting cell parameters and structural variables (*d, ϕ_1* and *ϕ_2*) of the computed minima are shown in Table S3. The notable differences in those parameters between the **1**-LT^{LS} and **1**-HT^{HS} minima are compatible with those observed between **1**-LT$_{X\text{-}ray}$ and **1**-HT$_{X\text{-}ray}$. Finally, it is worth noting that the **1**-LT^{HS} minimum has yielded unit-cell parameters and structural variables that lie between those of the **1**-LT^{LS} and **1**-HT^{HS} minima. In turn, for compound **2**, the only reported X-ray crystal structure was taken as starting structure for an optimization procedure on its LS and HS states, yielding the **2**^{LS} and **2**^{HS} minima, respectively (see Table S3).

Table S3. Unit cell parameters (*a*, *b*, *c*, α, β, γ) and main structural variables (*d*, ϕ_1, ϕ_2) of the Pair-I dimers in the reported X-ray crystal structures and in the computed minima of **1** and **2**.

	d (Å)	ϕ_1 (º)	ϕ_2 (º)	*a* (Å)	*b* (Å)	*c* (Å)	α (º)	β (º)	γ (º)
X-ray crystal structures									
1-LT$_{X\text{-}ray}$	3.50	78.8	75.6	8.11	8.65	9.47	80.5	67.8	90.2
1-HT$_{X\text{-}ray}$	3.73	70.6	81.8	8.25	8.61	9.52	79.8	67.1	86.5
2$_{X\text{-}ray}$	3.48	80.5	80.4	9.97	8.16	20.88	90.0	99.3	90.0
Minimum energy structures									
1-LT^{LS}	3.34	83.2	77.5	8.01	8.39	9.31	80.2	70.2	92.1
1-HT^{HS}	3.79	66.3	81.2	8.17	8.50	9.40	78.8	66.6	84.7
1-LT^{HS}	3.57	77.1	83.4	8.10	8.43	9.30	79.3	69.9	88.7
2^{LS}	3.33	81.7	82.9	8.83	7.02	18.32	90.0	99.8	90.0.
2^{HS}	3.52	78.8	82.9	8.77	7.20	18.09	90.0	99.2	90.0

Supp. Section S4 – Calculation of the magnetic exchange couplings

The Heisenberg Hamiltonian used throughout this paper is $\hat{H} = -2\sum J_{AB} \cdot \hat{S}_A \cdot \hat{S}_B$. The magnetic exchange coupling (J_{AB}) of the dimer of **1**-LT^{HS} (referred to as J_I) has been calculated at the B3LYP//6-311++g(d,p) level as implemented in Gaussian09.[6] The Broken Symmetry (BS) approach[7, 8] has been used to properly describe the open-shell low-spin state, together with the projection technique proposed by Yamaguchi and co-workers.[9] Note that we have selected the same method that was used for the calculation of the magnetic exchange couplings at the LT and HT crystal structures reported in ref. 9 of the main text.

Supp. Section S5 - Vibrational and electronic contributions to entropy

The importance of the vibrational and electronic contributions to entropy in driving the phase transition from LT to HT in compound **1** is analyzed in this section. At $T_{1/2}$, the free energy (*G*) of both phases is the same, so ΔG is equal to zero and one can write (eq.1):

$$\Delta S_{tot}(T_{1/2}) = \Delta H_{tot}(T_{1/2}) \quad (1)$$

Assuming that the contribution of the translational and rotational terms to total entropy is negligible, we can split this quantity into its electronic and vibrational components (eq. 2):

$$\Delta S_{tot}(T) = \Delta S_{elec} + \Delta S_{vib}(T) \quad (2)$$

The value of ΔS_{elec} can be considered to be temperature-independent and can be estimated using $\Delta S_{elec} = R \cdot \ln(2S+1)$, which corresponds to *ca.* 0.08 kcal·mol^{-1} at $T_{1/2}$= 60 K.[10] In turn, S_{vib} could be evaluated from *ab initio* calculations using the frequencies of the vibrational normal modes of the crystal (v_i). However, this would entail a huge computational effort (see Section S2) and, furthermore, small errors on the evaluation of v_i usually implies large deviations on S_{vib}, which would certainly put in doubt the accuracy of our estimation. In any case, following equations 1 and 2, and considering that ΔH is the adiabatic energy gap found between **1**-LT^{LS} and **1**-HT^{HS} (0.6 kcal·mol^{-1} per dimer), the contribution of vibrational entropy at $T_{1/2}$ would be *ca.* 0.52 kcal·mol^{-1} (0.6 − 0.08 kcal·mol^{-1} per dimer). Since this estimation depends strongly on the evaluation of ΔH, and it is expected that the

PBE-D2 method overestimates the stability of the LS state, we have performed a second estimation of S_{vib} using the normal modes of the singlet and triplet dimers in gas phase conditions (eq. 3).

$$S_{vib} = \sum_{i=1}^{N_{vib}} \left(\frac{h\nu_i}{T} \frac{1}{e^{h\nu_i/k_BT} - 1} - k_B ln\left(1 - e^{-h\nu_i/k_BT}\right) \right) \quad (3)$$

Using this strategy, we have found that the contribution of the vibrational entropy is 0.13 kcal·mol^{-1} per molecule. This value is in agreement with the expected overestimation of ΔH by the PBE functional. However, it becomes clear that vibrational entropy must be the main driving force in the phase transition of compound **1** (this has also been reported recently for the phase transitions of dithiazolyl-based radicals[11]). Nevertheless, as mentioned in the main text, the population of the HS state would be a necessary step to reach **1**-LT^{HS} and, eventually, **1**-HT^{HS}. Therefore, even though the vibrational entropy provides the thermodynamic stability of the HT phase in the high temperature regime, the phase transition occurs driven by the population of the HS state.

Supp. Section S6 – Computational details and structural information on the LS and HS minima of 1 and 2 calculated in the gas phase.

When working in gas phase conditions, the minimum energy structures of the HS (S=1) and LS (S=0) states of compounds **1**, **2** and **3** were obtained starting from the corresponding crystalline structures (when available) and using PBE-D2/TZVP as implemented in Gaussian09 package.[6]

In order to determine whether the energy barrier from **1**-LT^{LS} to **1**-HT^{HS} at the HS-PES is due to the constraints imposed by the crystal structure or, alternatively, due to the existence of two stable conformations of the dimer in the triplet state, we have performed geometry optimizations of the dimer in gas phase (*ie.* isolated pairs) conditions. Our calculations show that only one minimum exists for the HS state at gas phase and that its slippage is larger than the one obtained for the LS minimum (see Table 1 in the main text). Thus, this result indicates that the metastable **1**-LT^{HS} minimum exists due to the presence of an energy barrier originated on the intermolecular interactions between the columns of stacked radicals.

In order to rationalize the presence/absence of a second minimum in the HS-PES of **2**, optimizations of its dimer were performed in gas phase. Under these conditions, the crystal packing cannot be a source of constraints in the minimization procedure and, thus, a second minimum presenting larger slippage would be detected (if it exists). Those optimization procedures have been performed starting from the crystal structure of **2** in both the LS and HS states. We have further explored the HS-PES of **2** by means of multiple optimization procedures in which we have started from more slipped dimer structures, similar to those of the HS minima of compound **1**. After this inspection, only one LS and one HS minima have been found in the gas phase for compound **2**, whose characteristic geometrical parameters (*d, ϕ_1* and *ϕ_2*) are much similar than the ones shown between the HS and LS minima in compound **1** (see Table 1 in the main text).

Supp. Section S7 – Calculation and decomposition of interaction energies.

The nature of any intermolecular interaction can be determined by finding the dominant energetic component in an intermolecular perturbation theory (IMPT) analysis.[12] Assuming that the polarization and charge-transfer components of the IMPT interaction energy are 1 order of magnitude smaller than the remaining ones (as is usually done), the IMPT intermolecular interaction energy between two radicals, A and B, takes the following expression:[13]

$$E_{int} = E_{er} + E_{el} + E_{disp} + E_{bond} \quad (3)$$

where each term has the following physical meaning: (1) E_{er} is the exchange−repulsion energetic component that represents the repulsion that electrons feel when they occupy the same point of the space, according to the Pauli exclusion principle. This term is known to be proportional to the exponential of the overlap integral between the A and B wave functions; (2) E_{el} is the electrostatic energetic component, which can be accurately approximated as

the classic charge−charge interaction; (3) E_{disp} is the dispersion energetic component, a non-classical term that arises from the instantaneous dipole−dipole interactions resulting from the correlated motions of the electrons in A and B; (4) E_{bond} is the bonding energetic component, associated with the pairing, produced in the dimer, of the unpaired electrons of fragments A and B.

The total interaction energy (E_{int}) between the two monomers that form the dimer has been calculated as:

$$E_{int} = E_{dimer} - E_{monomer1} - E_{monomer2} \quad (5)$$

Then, the total interaction energy without the Grimme-D2 correction has been computed in order to evaluate the contribution of the dispersion term (E_{disp}). Since this correction is usually applied to improve the description of the dispersion interactions (*ie.* van der Waals interactions), the difference between the E_{int} when including or not Grimme-D2 correction can be roughly associated to the dispersion component. The bonding term E_{bond} originates from the paring component that is present when the dimer is found in the singlet state, and is strictly zero in the HS state. Consequently, it has been calculated as the vertical energy difference between both spin states at the each geometry. The electrostatic interaction (E_{el}) between the electron densities of the two monomers in the dimer has been approximately calculated as the sum of the classical charge-charge components by using the obtained optimum geometries and the atomic charges obtained within a NBO analysis[14] performed on the converged spin wave-functions. Finally the exchange-repulsion term E_{er} has been calculated as the difference between the total interaction energy and the previous dispersion, bonding and electrostatic terms. At this point, it must be stressed that our intention here has not been to obtain a quantitative estimation of all interactions but to have trends and, to this purpose, we believe that such estimation is sufficient. All energy evaluations have been performed at the B3LYP//6-311++g(d,p) level as implemented in Gaussian09.[6]

Apart from the two minima, we have also evaluated E_{int}, and the contribution of the different terms, in three more structures built by doing linear interpolation and extrapolation starting from the structures of the HS- and LS-minima. Therefore, the relative position of all atoms has been modified to obtain those structures. From this analysis, we can obtain clear picture of the E_{int} curves around the different spin-states minima (see Fig. S7a and Fig. S7b). First, the results show that, for each compound, the HS minima corresponds to the structural arrangements for which $E_{er} + E_{el} + E_{disp}$ is a minimum (see black line in Fig. S7a). In turn, the LS minima has the same $E_{er} + E_{el} + E_{disp}$ terms but also includes the bonding energy (E_{bond}). It must be noted that this drives the LS minima towards the structural arrangements for which E_{bond} is maximized, that is, towards slippage angles closer to 90 degrees (see red line in Fig. S7a). Second, the results also demonstrate that the difference in E_{int} between the compounds **1** and **2** (−23.3 vs. −27.2 kcal·mol^{-1} for the LS minima, see Table 1) must be associated mostly to a change in the strength of E_{disp} (−26.3 vs. −38.8 kcal·mol^{-1} for the LS minima, see Table 1).

Table 1. Contribution of the dispersion (E_{disp}), bonding (E_{bond}), electrostatic (E_{el}), and electron repulsion (E_{er}) terms to the total intermolecular interaction energies E_{int} (in kcal·mol^{-1}) at the HS and LS minima of compounds **1**, **2** and **3** calculated at the gas phase.

	Min.	E_{int}	E_{disp}	E_{bond}	E_{el}	E_{er}
1	**LS**	−23.3	−26.3	−2.0	−10.2	15.1
	HS	−22.5	−21.7	0.0	−10.0	9.3
2	**LS**	−27.2	−38.8	−1.9	2.5	11.0
	HS	−26.4	−35.2	0.0	3.2	5.6
3	**LS**	−22.0	−28.3	−1.5	−2.0	9.8
	HS	−21.7	−25.6	0.0	−2.4	6.3

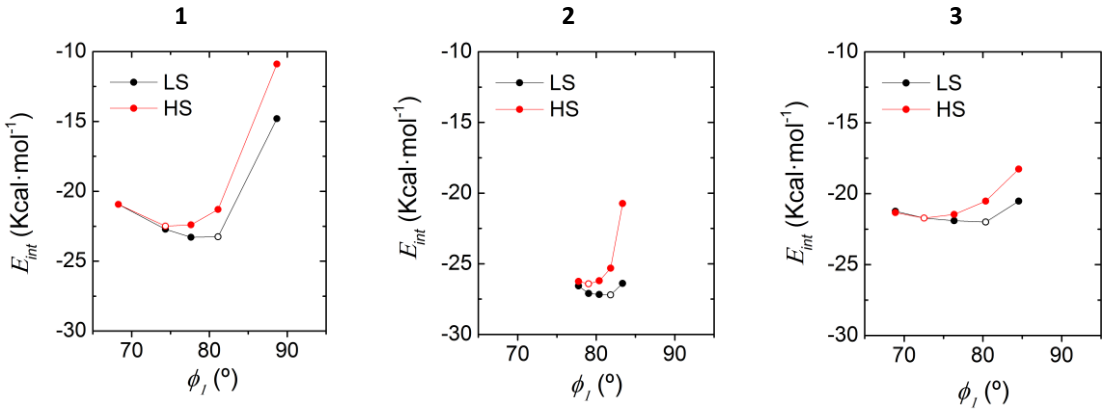

Figure S7a. Evolution of the interaction energies between monomers of compounds **1**, **2** and **3** along the structural distortion that connects the two minima, here represented by the slippage (longitudinal) angle ϕ_1. The open circles correspond to the position of the minima for each spin state.

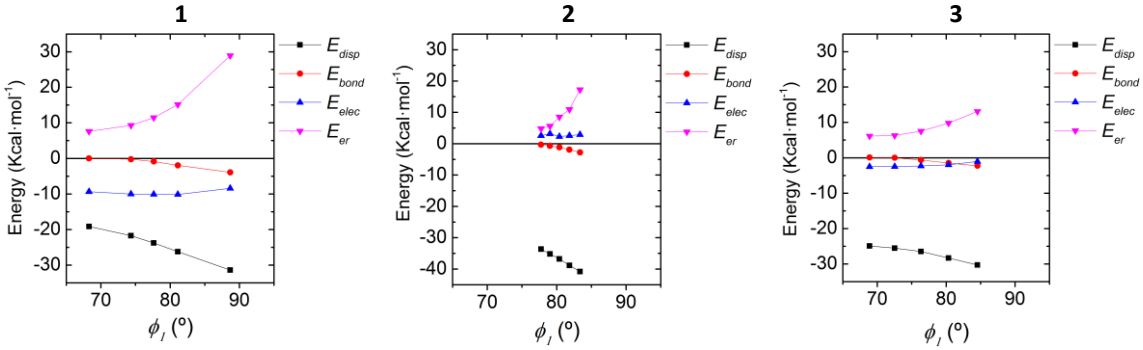

Figure S7b. Evolution of the dispersion (E_{disp}), electrostatic (E_{el}), Pauli exchange-repulsion (E_{er}) and bonding energy (E_{bond}) interactions between monomers of compounds **1**, **2** and **3** along the structural distortion that connects the two minima, here represented by the slippage (longitudinal) angle ϕ_1.

References

1. P. Giannozzi, S. Baroni, N. Bonini, M. Calandra, R. Car, C. Cavazzoni, D. Ceresoli, G. L. Chiarotti, M. Cococcioni, I. Dabo, A. D. Corso, S. d. Gironcoli, S. Fabris, G. Fratesi, R. Gebauer, U. Gerstmann, C. Gougoussis, A. Kokalj, M. Lazzeri, L. Martin-Samos, N. Marzari, F. Mauri, R. Mazzarello, S. Paolini, A. Pasquarello, L. Paulatto, C. Sbraccia, S. Scandolo, G. Sclauzero, A. P. Seitsonen, A. Smogunov, P. Umari and R. M. Wentzcovitch, *J. Phys.: Condens. Matter*, 2009, **21**, 395502.
2. J. P. Perdew, K. Burke and M. Ernzerhof, *Phys. Rev. Lett.*, 1997, **78**, 1396-1396.
3. J. P. Perdew, K. Burke and M. Ernzerhof, *Phys. Rev. Lett.*, 1996, **77**, 3865-3868.
4. S. Grimme, *J. Comput. Chem.*, 2006, **27**, 1787-1799.
5. T. Bucko, J. Hafner, S. Lebegue and J. G. Angyan, *J. Phys. Chem. A*, 2010, **114**, 11814-11824.
6. M. J. Frisch, G. W. Trucks, H. B. Schlegel, G. E. Scuseria, M. A. Robb, J. R. Cheeseman, G. Scalmani, V. Barone, B. Mennucci, G. A. Petersson, H. Nakatsuji, M. Caricato, X. Li, H. P. Hratchian, A. F. Izmaylov, J. Bloino, G. Zheng, J. L. Sonnenberg, M. Hada, M. Ehara, K. Toyota, R. Fukuda, J. Hasegawa, M. Ishida, T. Nakajima, Y. Honda, O. Kitao, H. Nakai, T. Vreven, J. A. Montgomery Jr., J. E. Peralta, F. Ogliaro, M. Bearpark, J. J. Heyd, E. Brothers, K. N. Kudin, V. N. Staroverov, R. Kobayashi, J. Normand, K. Raghavachari, A. Rendell, J. C. Burant, S. S. Iyengar, J. Tomasi, M. Cossi, N. Rega, J. M. Millam, M. Klene, J. E. Knox, J. B. Cross, V. Bakken, C. Adamo, J. Jaramillo, R. Gomperts, R. E. Stratmann, O. Yazyev, A. J. Austin, R. Cammi, C. Pomelli, J. W. Ochterski, R. L. Martin, K. Morokuma, V. G. Zakrzewski, G. A. Voth, P. Salvador, J. J. Dannenberg, S. Dapprich, A. D. Daniels, Ö. Farkas, J. B. Foresman, J. V. Ortiz, J. Cioslowski and D. J. Fox, 2009.
7. L. Noodleman and E. R. Davidson, *Chem. Phys.*, 1986, **109**, 131-143.
8. L. Noodleman, *J. Chem. Phys.*, 1981, **74**, 5737-5743.
9. T. Soda, Y. Kitagawa, T. Onishi, Y. Takano, Y. Shigeta, H. Nagao, Y. Yoshioka and K. Yamaguchi, *Chem. Phys. Lett.*, 2000, **319**, 223-230.
10. Note that this is the upper limit, obtained by considering that the J interactions are zero. In the current case, with small J values, $\Delta Selec$ would be slightly smaller

11. S. Vela, F. Mota, M. Deumal, R. Suizu, Y. Shuku, A. Mizuno, K. Awaga, M. Shiga, J. J. Novoa and J. Ribas-Arino, *Nat Commun*, 2014, **5**.
12. Hayes, I. C.; Stone, A. J. J. Mol. Phys. 1984, 53, 83.
13. Mota, F.; Miller, J. S.; Novoa, J. J., J. Am. Chem. Soc. 2009, 131, 7699.
14. Reed, A. E.; Curtiss, L. A.; Weinhold, F. Chem Rev 1988, 88, 899